CONFLUENTES MATHEMATICI

Roland BACHER

On geodesics of phyllotaxis

Tome 6, n° 1 (2014), p. 3-27.

<http://cml.cedram.org/item?id=CML_2014__6_1_3_0>

Confluentes Math.
6, 1 (2014) 3-27

ON GEODESICS OF PHYLLOTAXIS

ROLAND BACHER

Abstract. Seeds of sunflowers are often modelled by $n \longmapsto \varphi_\theta(n) = \sqrt{n}e^{2i\pi n\theta}$ leading to a roughly uniform repartition with seeds indexed by consecutive integers at angular distance $2\pi\theta$ for θ the golden ratio. We associate to such a map φ_θ a geodesic path $\gamma_\theta : \mathbb{R}_{>0} \longrightarrow \mathrm{PSL}_2(\mathbb{Z})\backslash\mathbb{H}$ of the modular curve and use it for local descriptions of the image $\varphi_\theta(\mathbb{N})$ of the phyllotactic map φ_θ.

Given a real parameter θ, we call the map $\varphi_\theta : \mathbb{N} \longrightarrow \mathbb{C}$ defined by

$$\varphi_\theta(n) = \sqrt{n}e^{2i\pi n\theta}$$

the *phyllotactic map of divergence angle* $2\pi\theta$ (measured in radians). The image $\varphi_\theta(\mathbb{N})$ of a phyllotactic map is the *phyllotactic set* (of parameter θ or divergence angle $2\pi\theta$). A phyllotactic set $\varphi_\theta(\mathbb{N})$ is uniformly discrete (i.e. two distinct elements of $\varphi_\theta(\mathbb{N})$ are at distance at least ϵ for some strictly positive ϵ) with uniform density if

$$\theta = [a_0; a_1, a_2, \dots] = a_0 + \cfrac{1}{a_1 + \frac{1}{a_2 + \dots}}$$

is irrational with bounded coefficients $a_0, a_1, a_2, \dots$ in its continued fraction expansion.

Among all possible parameters, the value given by the golden ratio $\frac{1+\sqrt{5}}{2} = [1; 1, 1, 1, \dots]$ (or closely related numbers) stands out and gives a particularly nice configuration. Figure 0.1 displays a few hundred small points of $\varphi_{(1+\sqrt{5})/2}(\mathbb{N})$.

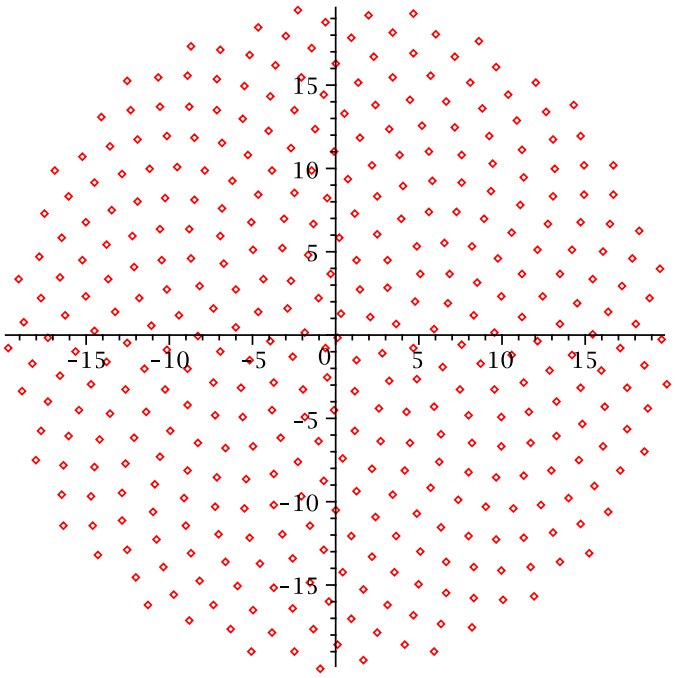

FIGURE 0.1. All points of $\varphi_{(1+\sqrt{5})/2}(\mathbb{N})$ in the disc $\{z \in \mathbb{C} \mid |z| \leqslant 20\}$.

Math. classification: 92B99, 11H31, 52C15.
Keywords: Lattice, hyperbolic geometry, phyllotaxis,sunflower-map.

Finite approximations of $\varphi_{(1+\sqrt{5})/2}(\mathbb{N})$ can be observed in capitula (heads) of sunflowers or daisies (the map $\varphi_{(1+\sqrt{5})/2}$, sometimes also called the sunflower-map, has been proposed in [16] as a model for heads of sunflowers). Joining close points of $\varphi_{(1+\sqrt{5})/2}(\mathbb{N})$ we get *parastichy spirals* appearing in pairs of crisscrossing families enumerated by two consecutive elements of the Fibonacci sequence $1, 2, 3, 5, 8, 13, 21, \ldots$. Explaining the occurence of the golden ratio and of Fibonacci numbers in botanics is the goal of phyllotaxis, see for example Chapter XIV of [15] or [6] for more recent developments.

Reasons for phyllotaxis should be separated from the mechanisms which are involved. How phyllotaxis works is surely best adressed by biologists, biochimists or biophysicists. The reason for phyllotaxis is efficiency of some sort (a precise definition is perhaps not so easy) which can take several forms. It is perhaps a physical notion like energetic efficiency or it involves geometric quantities like isoperimetry (which leads probably ultimately also to some kind of energetic efficiency). The link between the two aspects is natural selection. To say it in a nutshell, ubiquity of phyllotaxis involves mathematics: A few geometric configurations optimize some natural quantities. Thus they are favoured by living organisms through natural selection, see also Section 1.2 of [11] for a similar discussion.

Interestingly, the two aspects are spatially separated: Reasons for phyllotaxis, due to a globally optimized quantity, are of an asymptotical nature. They are best adressed by studying the large part of a plant which is relatively far from the central bud responsible for growth. Asymptotic arguments are thus not a weakness but are relevant when trying to understand the apparition of phyllotaxis in the course of evolution.

The aim of this paper is to describe an elegant framework involving hyperbolic geometry. More precisely, we approximate points of $\varphi_\theta(\mathbb{N})$ close to a given point $\varphi_\theta(n)$ using a sort of "linearization". This leads to an affine complex lattice. Each point of $\varphi_\theta(\mathbb{N})$ corresponds thus to a point of the modular curve parametrizing affine complex lattices, up to orientation-preserving affine similarities. It turns out that these points are on a geodesic of the modular curve which can be lifted to an explicit geodesic (depending only on θ and called the phyllotactic geodesic) of the Poincaré halfplane. The apparition of the golden ratio $\frac{1+\sqrt{5}}{2}$ (or of closely related numbers) as an optimal choice for θ is due to the fact that the corresponding phyllotactic geodesic accumulates to the shortest closed geodesic of the modular curve. It stays thus always far away from the cusp (corresponding to degenerate lattices) of the modular curve. This leads to good isoperimetric properties of the associated Voronoi domains and to economical forms of seeds in plants adopting such a divergence angle. Other features, such as the appearance of Fibonacci numbers enumerating families of parastichy spirals, are now simple geometric consequences.

The sequel of the paper is organized as follows:

Section 1 states the main result.

Section 2 contains useful (and probably mostly well-known) identities involving continuous fraction expansions.

Linearizations of phyllotactic sets are described in Section 3.

We construct the phyllotactic geodesic γ_θ in Section 4. This leads to a proof of Theorem 1.1.

Section 5 describes a different construction of a (slightly different) phyllotactic geodesic.

Section 6 is devoted to metric properties of phyllotactic sets.

Parastichy spirals are defined and studied in Section 7.

Section 8 describes a few combinatorial aspects of Voronoi diagrams for phyllotactic sets.

Section 9 discusses some chromatic aspects related to local canonical four-colourings of the Voronoi cells defined by phyllotactic sets.

Section 10 reviews briefly a few other models appearing in the literature.

Finally, Section 11 discusses a possible experimental verification (or refutation) of the existence of a phyllotactic geodesic in real sunflower-capitula.

Appendices contain basic definitions of hyperbolic geometry and of continued fractions.

1. Main result

Let (E, dist) be a metric space, x an element of E and ϵ, R two strictly positive real numbers. Two discrete subsets A, B of E are *ϵ-close in the open ball of radius R and center x* if there exists a map $\psi : A' \longrightarrow B'$ which is one-to-one and onto between subsets $A' \subset A$ and $B' \subset B$ containing all points in A, respectively B, at distance at most R from x and which moves all points of A' by less than ϵ, i.e. we have $\mathrm{dist}(a, \psi(a)) < \epsilon$ for all $a \in A'$. Intuitively, two discrete sets A, B are ϵ-close in the open ball of radius R centered at x if A and B are "equal up to an error of ϵ" in (a neighbourhood of) the ball of radius R centered at x.

Theorem 1.1. — *Given $\epsilon > 0$ and $R > 0$, there exists an integer $N = N(\epsilon, R)$ such that for every $\theta \in [0, 1)$ and for every $n \geqslant N$, the set $\varphi_\theta(\mathbb{N})$ is ϵ-close in the open disc of radius R centered at $\varphi_\theta(n)$ to an affine lattice in the equivalence class (i.e. up to orientation-preserving affine similarities) of $\mathbb{Z}+\mathbb{Z}\frac{4i\pi n}{1+4i\pi\{\theta\}n}$ (see Appendix A for reminders on complex lattices).*

The map

$$(0, \infty) \ni t \longmapsto \gamma_\theta(t) = \frac{4i\pi t}{1 + 4i\pi\{\theta\}t} = \frac{16\pi^2\{\theta\}t^2 + 4i\pi t}{1 + (4\pi\{\theta\}t)^2}$$

defines a geodesic of the hyperbolic Poincaré halfplane (endowed with the hyperbolic metric $\frac{ds}{y}$ at $z = x + iy \in \mathbb{H}$), see for example Lemma A.1. We call γ_θ the *phyllotactic geodesic* of φ_θ. Notice that the curve $t \longmapsto \gamma_\theta(t)$ has (hyperbolic) speed $\frac{1}{\Im(\gamma_\theta(t))}|\gamma'_\theta(t)| = \frac{1}{t}$ inversely proportional to t.

Remarks 1.2. —

(1) Theorem 1.1 holds for rational θ: In this case the phyllotactic geodesic ends up in the cusp of the modular curve $\mathrm{PSL}_2(\mathbb{Z})\backslash\mathbb{H}$. The associated affine lattices $\Lambda_{\theta,n}$ degenerate into discrete subgroups of rank 1 in the sense that they intersect a ball of fixed radius R centered at an affine lattice point along a translated copy of a discrete subgroup having rank 1.

(2) Denoting by $V(n)$ the Voronoi cell of $\varphi_\theta(n) \in \varphi_\theta(\mathbb{N})$, if θ is irrational we have $\lim_{n\to\infty} \mathrm{vol}V(n) = \pi$.

For rational $\theta = \frac{p}{q}$ with with $q \geqslant 3$ and p, q coprime integers, the union of Voronoi cells (defined by $\varphi_\theta(\mathbb{N})$) of all points at distance $\leqslant R$ from the origin is essentially a regular polygon with q sides and inradius R. This implies $\lim_{n\to\infty} \mathrm{vol}V(n) = q\tan\frac{\pi}{q} = \pi + \frac{\pi^3}{3q^2} + O\left(\frac{1}{q^4}\right)$.

For $\theta \in \frac{1}{2}\mathbb{Z}$, all Voronoi cells are unbounded and thus of infinite volume.

The existence of phyllotactic geodesics gives a measure of "similarity" of phyllotactic sets in neighbourhoods of $\varphi_\theta(n)$ and $\varphi_{\theta'}(m)$ by considering the hyperbolic distance $d_{\mathbb{H}}(\gamma_\theta(n), \mathrm{PSL}_2(\mathbb{Z})\gamma_{\theta'}(m))$ between the two orbits $\mathrm{PSL}_2(\mathbb{Z})\gamma_\theta(n)$ and $\mathrm{PSL}_2(\mathbb{Z})\gamma_{\theta'}(m)$. The last part of Remark 1.2 ensures that a small distance (with respect to $d_{\mathbb{H}}$) between $\gamma_\theta(n)$ and $\mathrm{PSL}_2(\mathbb{Z})\gamma_{\theta'}(m))$ implies the existence of bijections between $\varphi_\theta(\mathbb{N})$ and $\varphi_{\theta'}(\mathbb{N})$ which are almost isometries in neighbourhoods of $\varphi_\theta(n)$ and $\varphi_{\theta'}(m)$ if θ and θ' are irrational and have continued fraction-expansions with bounded coefficients. More generally, this holds if $\gamma_\theta(n)$ (and thus also $\gamma_{\theta'}(m)$) is far from the cusp of $\mathrm{PSL}_2(\mathbb{Z})\backslash\mathbb{H}$.

2. Useful identities for continued fractions

We collect here a few probably mostly well-known identities for continued fractions. Material of this Section, which can be skipped by the hurried reader, will only be used in some proofs.

Appendix B recalls basic definitions for continued fractions.

The following result is essentially identity 10.3.2 of [4]:

Proposition 2.1. — *We have*

$$\theta = \frac{p_{n-2} + \theta_n p_{n-1}}{q_{n-2} + \theta_n q_{n-1}}$$

for all $n \geqslant 0$.

Proof. — The result holds for $n = 0$.

We have

$$\begin{aligned} \frac{p_{n-1} + \theta_{n+1} p_n}{q_{n-1} + \theta_{n+1} q_n} &= \frac{p_{n-1} + \frac{1}{\theta_n - a_n}(p_{n-2} + a_n p_{n-1})}{q_{n-1} + \frac{1}{\theta_n - a_n}(q_{n-2} + a_n q_{n-1})} \\ &= \frac{p_{n-2} + \theta_n p_{n-1}}{q_{n-2} + \theta_n q_{n-1}} \end{aligned}$$

which ends the proof by induction. □

Lemma 2.2. — *We have*

$$\frac{\theta_{n+1}}{q_{n-1} + \theta_{n+1} q_n} = \frac{1}{q_{n-2} + \theta_n q_{n-1}} \ .$$

Proof. — We have

$$\begin{aligned} \frac{\theta_{n+1}}{q_{n-1} + \theta_{n+1} q_n} &= \frac{1}{\frac{1}{\theta_{n+1}} q_{n-1} + q_n} \\ &= \frac{1}{(\theta_n - a_n) q_{n-1} + q_n} \\ &= \frac{1}{\theta_n q_{n-1} - a_n q_{n-1} + q_{n-2} + a_n q_{n-1}} \end{aligned}$$

where we have used the recursive definitions $\frac{1}{\theta_{n+1}} = \theta_n - a_n$ and $q_n = q_{n-2} + a_n q_{n-1}$ of θ_{n+1} and of q_n. □

Proposition 2.3. — *We have*

$$\theta - \frac{p_{n-2} + x p_{n-1}}{q_{n-2} + x q_{n-1}} = \frac{(\theta_n - x)(-1)^n}{(q_{n-2} + x q_{n-1})(q_{n-2} + \theta_n q_{n-1})} \ . \tag{2.1}$$

Proof. — Proposition 2.1 shows that the result holds for $x = \theta_n$.

Since (2.1) is equivalent to the identity

$$(q_{n-2} + x q_{n-1})\theta - (p_{n-2} + x p_{n-1}) = \frac{\theta_n - x}{q_{n-2} + \theta_n q_{n-1}} (-1)^n \tag{2.2}$$

involving affine functions of x, it is enough to show the equality

$$q_{n-1}\theta - p_{n-1} = -\frac{(-1)^n}{q_{n-2} + \theta_n q_{n-1}} \ . \tag{2.3}$$

This holds for $n = 0$ since it boils down to $-1 = -1$. By induction, we have for $x = a_n$ the identity

$$\theta - \frac{p_{n-2} + a_n p_{n-1}}{q_{n-2} + a_n q_{n-1}} = \frac{(\theta_n - a_n)(-1)^n}{(q_{n-2} + a_n q_{n-1})(q_{n-2} + \theta_n q_{n-1})}$$

which can be rewritten as

$$\theta - \frac{p_n}{q_n} = \frac{(-1)^n}{\theta_{n+1} q_n (q_{n-2} + \theta_n q_{n-1})} \tag{2.4}$$

using the recursive definitions of $p_n,\ q_n$ and θ_{n+1}.

The identity

$$\theta_{n+1}\left(q_{n-2}+\theta_n q_{n-1}\right)=q_{n-1}+\theta_{n+1}q_n$$

equivalent to Lemma 2.2 yields now (2.3) for $n+1$. □

Remark 2.4. — Identity (2.4) (corresponding to the specialization $x=a_n$ of Proposition 2.3) strengthens inequality (B.3) since $a_{n+1}=\lfloor\theta_{n+1}\rfloor\leqslant\theta_{n+1}$ and $q_n=q_{n-2}+a_nq_{n-1}\leqslant q_{n-2}+\theta_nq_{n-1}$.

Lemma 2.5. — *We have*

$$\frac{1}{q_{n-2}+\theta_nq_{n-1}}-\frac{a_{n+1}}{q_{n-1}+\theta_{n+1}q_n}=\frac{1}{q_n+\theta_{n+2}q_{n+1}}\ .$$

Proof. — Using the identities

$$\begin{aligned}q_k&=q_{k-2}+a_kq_{k-1},\\ \theta_{k+1}&=\frac{1}{\theta_k-a_k},\end{aligned}$$

for $k=n$ and $k=n+1$ we have

$$\begin{aligned}&\frac{1}{q_{n-2}+\theta_nq_{n-1}}-\frac{a_{n+1}}{q_{n-1}+\theta_{n+1}q_n}\\ &=\frac{1}{q_n-a_nq_{n-1}+\theta_nq_{n-1}}-\frac{a_{n+1}}{q_{n-1}+\theta_{n+1}q_n}\\ &=\frac{1}{q_n+\frac{1}{\theta_{n+1}}q_{n-1}}-\frac{a_{n+1}}{q_{n-1}+\theta_{n+1}q_n}\\ &=\frac{\theta_{n+1}-a_{n+1}}{q_{n-1}+\theta_{n+1}q_n}\\ &=\frac{\theta_{n+1}-a_{n+1}}{q_{n-1}+a_{n+1}q_n+(\theta_{n+1}-a_{n+1})q_n}\\ &=\frac{1}{\theta_{n+2}q_{n+1}+q_n}\end{aligned}$$

which ends the proof. □

3. Linearization

Proposition 3.1. — *We have*

$$\begin{aligned}\varphi_\theta(n+aq_{j-1}+bq_j)-\varphi_\theta(n)&=a\left(\frac{q_{j-1}}{2\sqrt{n}}-\frac{(-1)^j2i\pi\sqrt{n}\theta_{j+1}}{q_{j-1}+\theta_{j+1}q_j}\right)e^{2i\pi n\theta}\\ &\quad+b\left(\frac{q_j}{2\sqrt{n}}+\frac{(-1)^j2i\pi\sqrt{n}\theta_{j+2}}{q_j+\theta_{j+2}q_{j+1}}\right)e^{2i\pi n\theta}\\ &\quad+E_j(a,b)\end{aligned}$$

where q_k is the denominator of the k-th convergent $\frac{p_k}{q_k}=[a_0;a_1,\dots,a_k]$ for $\theta=[a_0;a_1,a_2,\dots]$, where $\theta_k=[a_k;a_{k+1},a_{k+2},\dots]$ and where the error $E_j(a,b)$ is asymptotically given by

$$\left(\tfrac{-1}{8n^{3/2}}(aq_{j-1}+bq_j)^2+\tfrac{i\pi}{\sqrt{n}}(aq_{j-1}+bq_j)\delta-2\pi^2\sqrt{n}\delta^2\right)e^{2i\pi n\theta}$$

with

$$\delta=-a\frac{(-1)^j\theta_{j+1}}{q_{j-1}+\theta_{j+1}q_j}+b\frac{(-1)^j\theta_{j+2}}{q_j+\theta_{j+2}q_{j+1}}$$

if $|\varphi_\theta(n+aq_{j-1}+bq_j)-\varphi_\theta(n)|=O(1)$.

Corollary 3.2. — *If q_{j-1} and q_j are denominators of two consecutive convergents $\frac{p_{j-1}}{q_{j-1}}$ and $\frac{p_j}{q_j}$ of θ such that $q_{j-1} \leqslant \sqrt{n} < q_j$, then the smallest points of*

$$(\varphi_\theta(\mathbb{N}) - \varphi_\theta(n))\, e^{-2i\pi n\theta}$$

are close to the smallest points of the lattice

$$\mathbb{Z}\left(\frac{q_{j-1}}{2\sqrt{n}} - (-1)^j \frac{2i\pi\sqrt{n}\theta_{j+1}}{q_{j-1}+\theta_{j+1}q_j}\right) + \mathbb{Z}\left(\frac{q_j}{2\sqrt{n}} + (-1)^j \frac{2i\pi\sqrt{n}\theta_{j+2}}{q_j+\theta_{j+2}q_{j+1}}\right) \qquad (3.1)$$

with an error of order $O\left(\frac{1}{\sqrt{n}}\right)$.

The lattice described by (3.1) contains always a non-zero element of absolute value smaller than $\sqrt{\frac{1}{4}+4\pi^2} < 3\pi$.

Remark 3.3. — Fundamental domains of the lattice Λ given by (3.1) have area π as shown by the identities

$$\begin{array}{rcl}
(-1)^j \det \begin{pmatrix} \frac{q_{j-1}}{2\sqrt{n}} & -\frac{(-1)^j 2i\pi\sqrt{n}\theta_{j+1}}{q_{j-1}+\theta_{j+1}q_j} \\ \frac{q_j}{2\sqrt{n}} & +\frac{(-1)^j 2i\pi\sqrt{n}\theta_{j+2}}{q_j+\theta_{j+2}q_{j+1}} \end{pmatrix} & & \\
= & \left(q_{j-1}\dfrac{\theta_{j+2}}{q_j+\theta_{j+2}q_{j+1}} + q_j\dfrac{\theta_{j+1}}{q_{j-1}+\theta_{j+1}q_j}\right)\pi & \\
= & \left(q_{j-1}\dfrac{1}{q_{j-1}+\theta_{j+1}q_j} + q_j\dfrac{\theta_{j+1}}{q_{j-1}+\theta_{j+1}q_j}\right)\pi & \\
= & \pi &
\end{array}$$

where the second equality is given by Lemma 2.2.

Since the regular hexagonal lattice has maximal density, the lattice Λ contains always a non-zero element of absolute value at most $\sqrt{\frac{2\pi}{\sqrt{3}}} \sim 1.9046$.

Proof of Proposition 3.1. — Setting

$$F(s,\gamma) = \sqrt{n+s}\; e^{2i\pi n\theta + 2i\pi\gamma}$$

we want to approximate

$$F(aq_{j-1}+bq_j, \delta) - F(0,0)$$

where $\delta = (aq_{j-1}+bq_j)\theta - c$ is the difference between $(aq_{j-1}+bq_j)\theta$ and the integer c closest to $(aq_{j-1}+bq_j)\theta$. We proceed in the usual way by considering the linear approximation

$$L = \frac{\partial F}{\partial s}(0,0)(aq_{j-1}+bq_j) + \frac{\partial F}{\partial \gamma}(0,0)\delta$$

and by estimating the error using second-order derivatives. The necessary partial derivatives of F are:

$$\begin{array}{rcl}
\dfrac{\partial F}{\partial s}(0,0) & = & \dfrac{1}{2\sqrt{n}} e^{2i\pi n\theta}, \\
\dfrac{\partial F}{\partial \gamma}(0,0) & = & 2i\pi\sqrt{n} e^{2i\pi n\theta}, \\
\dfrac{\partial^2 F}{\partial s^2}(0,0) & = & \dfrac{-1}{4n^{3/2}} e^{2i\pi n\theta}, \\
\dfrac{\partial^2 F}{\partial s \partial \gamma}(0,0) & = & \dfrac{i\pi}{\sqrt{n}} e^{2i\pi n\theta}, \\
\dfrac{\partial^2 F}{\partial \gamma^2}(0,0) & = & -4\pi^2\sqrt{n} e^{2i\pi n\theta}.
\end{array}$$

The contribution coming from $\frac{\partial F}{\partial s}(0,0)(aq_{j-1}+bq_j)$ to L is given by

$$\frac{1}{2\sqrt{n}}e^{2i\pi n\theta}(aq_{j-1}+bq_j)\ .$$

In order to compute $\frac{\partial F}{\partial \gamma}(0,0)\delta$ we split δ into $\delta = a\delta_{j-1}+b\delta_j$ where δ_k for $k\in\{j-1,j\}$ is the difference between $q_k\theta$ and the integer closest to $q_k\theta$. Since q_k is a denominator of the convergent $\frac{p_k}{q_k}=[a_0;a_1,\dots,a_k]$ of θ, this integer is given by the numerator p_k. We have

$$\begin{aligned}\theta-\frac{p_k}{q_k} &= \frac{p_k+\theta_{k+2}p_{k+1}}{q_k+\theta_{k+2}q_{k+1}}-\frac{p_k}{q_k}\\ &= \frac{(p_{k+1}q_k-p_kq_{k+1})\theta_{k+2}}{q_k(q_k+\theta_{k+2}q_{k+1})}\\ &= (-1)^k\frac{\theta_{k+2}}{q_k(q_k+\theta_{k+2}q_{k+1})}\end{aligned}$$

where we have used Proposition 2.1 and the well-known identity $p_{k+1}q_k-p_kq_{k+1}=(-1)^k$ (see equality (B.2) of Appendix B). This yields

$$\delta_k=(-1)^k\frac{\theta_{k+2}}{q_k+\theta_{k+2}q_{k+1}}$$

and shows

$$\begin{aligned}\frac{\partial F}{\partial s}(0,0)\delta &= \frac{\partial F}{\partial s}(0,0)(a\delta_{j-1}+b\delta_j)\\ &= \frac{\partial F}{\partial s}(0,0)\left(-a\frac{(-1)^j\theta_{j+1}}{q_{j-1}+\theta_{j+1}q_j}+b\frac{(-1)^j\theta_{j+2}}{q_j+\theta_{j+2}q_{j+1}}\right).\end{aligned}$$

The order of the error is given by

$$\frac{1}{2}\frac{\partial^2 F}{\partial s^2}(0,0)(aq_{j-1}+bq_j)^2+\frac{\partial^2 F}{\partial s\partial\gamma}(0,0)(aq_{j-1}+bq_j)\delta+\frac{1}{2}\frac{\partial^2 F}{\partial\gamma^2}(0,0)\delta^2$$

and can be evaluated easily. □

4. The phyllotactic geodesic and proof of Theorem 1.1

Using (2.2) we can rewrite the lattice Λ given by formula (3.1) of Corollary 3.2 as

$$\mathbb{Z}\left(\frac{q_{j-1}}{2\sqrt{n}}-(-1)^j\frac{2i\pi\sqrt{n}}{q_{j-2}+\theta_jq_{j-1}}\right)+\mathbb{Z}\left(\frac{q_j}{2\sqrt{n}}+(-1)^j\frac{2i\pi\sqrt{n}}{q_{j-1}+\theta_{j+1}q_j}\right)\ .$$

In particular, the lattice Λ is similar to the lattice $\mathbb{Z}+\mathbb{Z}\tau_j(n)$ where

$$\tau_j(t)=-(-1)^j\frac{q_{j-1}-(-1)^j\frac{4i\pi t}{q_{j-2}+\theta_jq_{j-1}}}{q_j+(-1)^j\frac{4i\pi t}{q_{j-1}+\theta_{j+1}q_j}}\ . \tag{4.1}$$

Remark 4.1. — A straightforward computation shows that the imaginary part of $\tau_j(t)$, given by

$$\frac{\frac{q_{j-1}}{q_{j-1}+\theta_{j+1}q_j}+\frac{q_j}{q_{j-2}+\theta_jq_{j-1}}}{q_j^2+\frac{16\pi^2t^2}{(q_{j-1}+\theta_{j+1}q_j)^2}}4\pi t\ ,$$

is strictly positive if t is strictly positive.

Theorem 4.2. — *For all $j\geqslant 0$ we have*

$$(\tau_j(t)-(-1)^ja_{j+1})\tau_{j+1}(t)=-1\ .$$

Proof. — Theorem 4.2 boils down to the identity

$$\begin{aligned} & q_{j-1} - (-1)^j \frac{4i\pi t}{q_{j-2} + \theta_j q_{j-1}} + a_{j+1} q_j + a_{j+1} (-1)^j \frac{4i\pi t}{q_{j-1} + \theta_{j+1} q_j} \\ = \quad & q_{j+1} - (-1)^j \frac{4i\pi t}{q_j + \theta_{j+2} q_{j+1}} \ . \end{aligned}$$

The identity $q_{j+1} = q_{j-1} + a_{j+1} q_j$ shows that the constant parts (with respect to t) of both sides are equal. Linear coefficients of t are equal by Lemma 2.5. □

Proof of Theorem 1.1. — By Theorem 4.2, the two geodesics defined by τ_j and τ_{j+1} are related by the integral Möbius transformations

$$\tau_{j+1} = \frac{-1}{\tau_j - (-1)^j a_{j+1}} = \begin{pmatrix} 0 & 1 \\ -1 & (-1)^j a_{j+1} \end{pmatrix} \cdot \tau_j \tag{4.2}$$

and

$$\tau_j = \frac{(-1)^j a_{j+1} \tau_{j+1} - 1}{\tau_{j+1}} = \begin{pmatrix} (-1)^j a_{j+1} & -1 \\ 1 & 0 \end{pmatrix} \cdot \tau_{j+1} \ . \tag{4.3}$$

Thus they project onto a unique geodesic on the modular curve $\mathrm{PSL}_2(\mathbb{Z})\backslash\mathbb{H}$ represented for example by

$$\tau_0(t) = -\frac{q_{-1} - \frac{4i\pi t}{q_{-2} + \theta_0 q_{-1}}}{q_0 + \frac{4i\pi t}{q_{-1} + \theta_1 q_0}} = \frac{4i\pi t}{1 + \frac{4i\pi t}{\theta_1}} = \frac{4i\pi t}{1 + 4i\pi \{\theta\} t} \tag{4.4}$$

(where $q_{-2} = 1,\ q_{-1} = 0,\ q_0 = 1$ and $\theta_1 = \frac{1}{\theta - a_0} = \frac{1}{\{\theta\}}$).

This implies Theorem 1.1 since the linearization error is of order $O\left(\frac{1}{\sqrt{n}}\right)$ for elements of $\varphi_\theta(\mathbb{N})$ at bounded distance from $\varphi_\theta(n)$. □

Formula (4.4) defines a geodesic of the hyperbolic half-plane for every real number θ. Indeed, (4.4) is a vertical half-line (and thus a hyperbolic geodesic) if θ is integral and it defines a halfcircle of $\mathbb{H}$ orthogonal to $\mathbb{R}$ (and thus a geodesic) with boundary points 0 corresponding to $t = 0$ and $\frac{1}{\{\theta\}}$ corresponding to $t = \infty$ otherwise.

Diophantine properties of θ are related to the dynamical behaviour of the geodesic γ_θ projected onto $\mathrm{PSL}_2(\mathbb{Z})\backslash\mathbb{H}$, see [13] which describes some closely related dynamics. More precisely, (the projection of) the geodesic γ_θ, after starting at the cusp, turns a_1 times around the cusp before passing between the two conical points of the modular curve. It turns then a_2 times around the cusp before crossing again the shortest geodesic segment joining the two conical points and so on. A large coefficient a_k causes the (projection of the) geodesic γ_θ to climb the modular curve up to a height given asymptotically (in a_k) by $a_k i \in \mathcal{M}$. This gives rise to points of $\varphi_\theta(\mathbb{N})$ having Voronoi cells with bad isoperimetric properties.

For a divergence angle $2\pi\theta$ determined by the golden ratio $\theta = \frac{1+\sqrt{5}}{2}$ (or close relatives of it) the continued fraction expansion involves only ones (or only ones after perhaps a few initial "accidents"). This is the optimal situation leaving no possibility of improvement. In particular, the phyllotactic geodesic $\gamma_{(1+\sqrt{5})/2}$ is asymptotically equal to the geodesic

$$t \longmapsto \tilde{\gamma}(t) = \frac{(-1+\sqrt{5})it - 1 - \sqrt{5}}{2(it+1)} = \frac{-1-\sqrt{5} + (-1+\sqrt{5})t^2 + 2it\sqrt{5}}{2(1+t^2)}$$

with boundary points $\frac{-1\pm\sqrt{5}}{2}$ (and containing the points $-1+i = \tilde{\gamma}\left(\frac{-1+\sqrt{5}}{2}\right)$ and $i = \tilde{\gamma}\left(\frac{1+\sqrt{5}}{2}\right)$ of $\mathbb{H}$). The equality

$$\tilde{\gamma}(\theta^4 t) = \frac{\tilde{\gamma}(t) + 1}{\tilde{\gamma}(t) + 2}$$

shows that $\tilde{\gamma}$ is invariant under the integral Möbius transformation defined by the matrix

$$\begin{pmatrix} 1 & 1 \\ 1 & 2 \end{pmatrix} = \begin{pmatrix} 0 & 1 \\ 1 & 1 \end{pmatrix}^2 .$$

It projects onto the shortest closed geodesic of the modular curve $\mathrm{PSL}_2(\mathbb{Z})\backslash\mathbb{H}$.

Since $\frac{d}{dt}\tilde{\gamma}(t) = \frac{-\sqrt{5}}{(t-i)^2}$, the parametrized geodesic $\tilde{\gamma}(t)$ has the same instant speed $\frac{1}{\Im(\tilde{\gamma}(t))}|\tilde{\gamma}'(t)| = \frac{1}{t}$ as the phyllotactic geodesic $\gamma_\theta(t)$. We have thus asymptotically $\gamma_\theta(t) \sim \gamma_\theta\left(\theta^4 t\right)$. The phyllotactic set $\varphi_\theta(\mathbb{N})$ has thus almost isometrical neighbourhoods around $\varphi_\theta(n)$ and $\varphi_\theta(m)$ if n is large and m is close to $\theta^4 n$.

5. A geometric construction

We construct in this section a slightly different geodesic (asymptotically associated to linearizations of $\varphi_\theta(\mathbb{N})$) of the modular domain $\mathrm{PSL}_2(\mathbb{Z})\backslash\mathbb{H}$.

We denote by $\mathcal{L} = \mathcal{L}_\theta$ the line $\mathbb{R}(1, -\theta)$ of slope $-\theta$ containing the origin. A convergent $\frac{p_j}{q_j} = [a_0; a_1, \ldots, a_j]$ of $\theta = [a_0; a_1, a_2, \ldots]$ yields an integral point $(q_j, -p_j)$ close to $\mathcal{L}$ as follows: Denoting by $\pi_{\mathcal{L}}(q_j, -p_j)$ the orthogonal projection of $(q_j, -p_j)$ onto $\mathcal{L}$ we have

$$\pi_{\mathcal{L}}(q_j, -p_j) = q_j(1, -\theta) + O\left(\frac{1}{q_j}\right)(1, -\theta)$$

for all $j \geqslant 0$. The equality $q_j\theta - p_j = (-1)^j \frac{\theta_{j+2}}{q_j + \theta_{j+2}q_{j+1}}$ corresponding to the case $n = j + 2$ and $x = 0$ of Proposition 2.3 implies the identity

$$(q_j, -p_j) - q_j(1, -\theta) = \left(0, (-1)^j \frac{\theta_{j+2}}{q_j + \theta_{j+2}q_{j+1}}\right) .$$

The orthogonal projection $\pi_{\mathcal{L}^\perp}(q_j, -p_j)$ of $(q_j, -p_j)$ onto the line $\mathcal{L}^\perp = \mathbb{R}(\theta, 1)$ orthogonal to $\mathcal{L} = \mathbb{R}(1, -\theta)$ is given by

$$\begin{aligned} \pi_{\mathcal{L}^\perp}(q_j, -p_j) &= \pi_{\mathcal{L}^\perp}\big((q_j, -p_j) - q_j(1, -\theta)\big) \\ &= \frac{(-1)^j\theta_{j+2}}{(q_j + \theta_{j+2}q_{j+1})} \frac{(\theta, 1)}{(1 + \theta^2)} . \end{aligned}$$

Thus we can rewrite the right side of the obvious identity

$$(q_j, -p_j) = \pi_{\mathcal{L}}(q_j, -p_j) + \pi_{\mathcal{L}^\perp}(q_j, -p_j)$$

as

$$q_j(1, -\theta) + \frac{(-1)^j 4\pi n\theta_{j+2}}{(q_j + \theta_{j+2}q_{j+1})} \frac{(\theta, 1)}{4\pi n(1 + \theta^2)} + O\left(\frac{1}{q_j}\right)(1, -\theta) . \tag{5.1}$$

We endow now $\mathbb{R}^2$ with an Euclidean metric $ds_{\theta,n}$ turning the vectors

$$(1, -\theta), \quad \frac{(\theta, 1)}{4\pi n(1 + \theta^2)}$$

into an orthogonal basis. Comparision of (5.1) with (3.1) shows that the lattice $(\mathbb{Z}^2, ds_{\theta,n})$ is asymptotically equivalent with the linearization of $\varphi_\theta(\mathbb{N})$ at the point $\varphi_\theta(n)$. Since

$$\begin{aligned} (1, 0) &= \frac{1}{1 + \theta^2}(1, -\theta) + 4\pi n\theta \frac{(\theta, 1)}{4\pi n(1 + \theta^2)}, \\ (0, 1) &= -\frac{\theta}{1 + \theta^2}(1, -\theta) + 4\pi n \frac{(\theta, 1)}{4\pi n(1 + \theta^2)}, \end{aligned}$$

the Euclidean lattice $(\mathbb{Z}^2, ds_{\theta,n})$ corresponds to the point of $\mathrm{PSL}_2(\mathbb{Z})\backslash\mathbb{H}$ represented by

$$\begin{aligned} & \frac{1+4i\pi n\theta(1+\theta^2)}{\theta-4i\pi n(1+\theta^2)} \\ = \quad & \frac{\theta-16\pi^2n^2\theta(1+\theta^2)^2+4i\pi n(1+\theta^2)^2}{\theta^2+16\pi^2n^2(1+\theta^2)^2}\ . \end{aligned}$$

All these points are elements of the hyperbolic geodesic with boundary points $\frac{1}{\theta}$ (for $n=0$) and $-\theta = \begin{pmatrix} a_0 & 1 \\ -1 & 0 \end{pmatrix} \frac{1}{\{\theta\}}$ (for $n=\infty$).

Remark 5.1. — Since we have

$$\begin{aligned} & \frac{1+4i\pi t\theta(1+\theta^2)}{\theta-4i\pi t(1+\theta^2)} - \begin{pmatrix} a_0 & 1 \\ -1 & 0 \end{pmatrix} \frac{4i\pi t}{4i\pi\{\theta\}t+1} \\ = \quad & \frac{1+4i\pi t\theta(1+\theta^2)}{\theta-4i\pi t(1+\theta^2)} + \frac{4i\pi\theta t+1}{4i\pi t} \\ = \quad & \frac{\theta}{4i\pi t(\theta-4i\pi t(1+\theta^2))} \\ = \quad & \frac{1+\theta^2}{\theta^2+16\pi^2t^2(1+\theta^2)^2} - \frac{\theta^2}{4\pi t\left(\theta^2+16\pi^2t^2(1+\theta^2)^2\right)}i\ , \end{aligned}$$

the hyperbolic distance between the two points

$$\frac{1+4i\pi t\theta(1+\theta^2)}{\theta-4i\pi t(1+\theta^2)} \text{ and } \begin{pmatrix} a_0 & 1 \\ -1 & 0 \end{pmatrix} \frac{4i\pi t}{4i\pi\{\theta\}t+1}$$

of $\mathbb{H}$ is roughly given by

$$\frac{\theta^2+16\pi^2t^2(1+\theta^2)^2}{4\pi t(1+\theta^2)^2} \left| \frac{1+\theta^2}{\theta^2+16\pi^2t^2(1+\theta^2)^2} - \frac{\theta^2}{4\pi t\left(\theta^2+16\pi^2t^2(1+\theta^2)^2\right)}i \right|$$

which simplifies to

$$\left| \frac{1}{4\pi t(1+\theta^2)} - \frac{\theta^2}{16\pi^2t^2}i \right|\ .$$

Thus it is asymptotically equal to $\frac{1}{4\pi t(1+\theta^2)}$ which is asymptotically much smaller than the error $O\left(\frac{1}{\sqrt{n}}\right)$ due to linearization at a point $\varphi_\theta(n) = \sqrt{n}e^{2i\pi\theta n}$ of order $O(\sqrt{n})$.

6. Metric properties of phyllotactic sets

A subset S of a metric space E is *uniformly discrete* if there exists a strictly positive real constant δ such that $d(a,b) \geqslant \delta$ for every pair a, b of distinct points in S. Equivalently, S is uniformly discrete if open balls of radius $\delta/2$ centered at all elements of E are disjoint (for a small strictly positive constant δ).

A subset $\mathcal{S}$ of a metric space E is an *ϵ-net* if every point of E is at distance at most ϵ from a point of $\mathcal{S}$. Equivalently, E is covered by the set of closed balls of radius ϵ centered at elements of $\mathcal{S}$.

The following result is a straightforward consequence of the fact that areæ of Voronoi cells defined by $\varphi_\theta(\mathbb{N})$ are asymptotically equal to π if θ is irrational:

Proposition 6.1. — *The following assertions are equivalent:*

(i) θ is irrational and has bounded coefficients $a_1, a_2, \ldots$ in its continued fraction expansion $\theta = [a_0; a_1, a_2, \ldots]$.

(ii) $\varphi_\theta(\mathbb{N})$ is uniformly discrete in $\mathbb{C}$ (identified with the Euclidean plane in the obvious way).

(iii) $\varphi_\theta(\mathbb{N})$ is an ϵ-net of $\mathbb{C}$.

(iv) All Voronoi cells of $\varphi_\theta(\mathbb{N})$ have bounded diameter.

(v) Discs of radius R (and arbitrary centers) in $\mathbb{C}$ contain $R(R+O(1))$ points of $\varphi_\theta(\mathbb{N})$.

(vi) The image $\gamma_\theta([1,\infty))$ of the phyllotactic "half-geodesic" is contained in a compact subset of the modular curve $\mathrm{PSL}_2(\mathbb{Z})\backslash\mathbb{H}$.

We leave the proof to the reader. □

Observe that $\varphi_\theta(\mathbb{N})$ is never uniformly discrete if θ is rational.

7. Parastichy spirals

We denote by $\partial\mathcal{M}$ the boundary in $\mathbb{C}$ of the fundamental domain $\mathcal{M}$ defined by (A.1). The interior $\mathcal{M}\setminus\partial\mathcal{M}$ corresponds to lattices having a unique pair $\pm u$ of opposite shortest non-zero vectors and a unique pair $\pm v$ of shortest vectors which are $\mathbb{R}$-linearly independent from $\pm u$. More precisely, for $z\in\mathcal{M}\setminus\partial\mathcal{M}$ the unique pair $\pm u$ of non-zero shortest vectors in $\mathbb{Z}+\mathbb{Z}z$ is given by ± 1 and the unique pair $\pm v$ of shortest vectors outside $\mathbb{R}$ coincides with $\pm z$. Notice that $\mathbb{R}$-linear independency of v from u is necessary in order to discard $\pm 2u, \pm 3u, \dots$ which might be smaller than v for lattices associated to $z\in\mathcal{M}$ with large modulus.

Lattices corresponding to elements z of norm 1 in $\mathcal{M}$ have (at least) two pairs of shortest vectors given by ± 1 and $\pm z$ in $\mathbb{Z}+\mathbb{Z}z$. The regular hexagonal lattice corresponding to $z=\frac{1+i\sqrt{3}}{2}$ is the unique lattice with three pairs $\pm 1, \pm\frac{1+i\sqrt{3}}{2}, \pm\frac{1-i\sqrt{3}}{2}$ of shortest non-zero vectors. Lattices associated to $z=\frac{1+it}{2}$ for $t>\sqrt{3}$ have a unique pair ± 1 of shortest non-zero-vectors and two non-real pairs $\pm z$ and $\pm(z-1)$ of shortest non-real vectors.

Connecting points of a lattice Λ indexed by $z\in\mathcal{M}\setminus\partial\mathcal{M}$ with their closest neighbours we get a set of parallel lines. Joining closest lattice-points on two such adjacent lines we obtain a second set of parallel lines. These two sets of parallel lines cut the complex plane into fundamental domains for Λ given by isometric rhombi.

Parastichy spirals are analogues of these lines in $\varphi_\theta(\mathbb{N})$. More precisely, we define (generically) the *primary parastichy spirals* of $\varphi_\theta(\mathbb{N})$ as the piecewise-wise linear paths obtained by joining vertices of $\varphi_\theta(\mathbb{N})$ to their two approximatively opposite nearest neighbours. Similarly, we construct *secondary parastichy spirals* by joining vertices of $\varphi_\theta(\mathbb{N})$ to their nearest neighbours on adjacent neighbouring primary parastichy spirals.

Primary parastichy spirals exist essentially at every point far from the origin except where they become blurred with secondary parastichy spirals. At such points (corresponding to crossings of the phyllotactic geodesic with the image of the unit circle in $\mathrm{PSL}_2(\mathbb{Z})\backslash\mathbb{H}$), primary and secondary parastichy spirals get exchanged. We call such a situation a *parastichy transition of type I*.

Secondary parastichy spirals are however well-defined only if the local situation corresponds to a lattice indexed by an element of $\mathcal{M}$ which is not too close to the cusp. For example, the phyllotactic set $\varphi_\theta(\mathbb{N})$ associated to a rational number $\theta=\frac{p}{q}$ is contained in q half-rays originating at 0. Far from the origin, primary parastichies coincide with these half-rays (and are no longer spirals) and secondary parastichies make no longer sense. Moreover, for points $z\in\mathcal{M}$ with real part close to $1/2$ (or $-1/2$) a family of secondary parastichy spirals fades away and is replaced by a new family of secondary parastichy spirals, giving rise to a *parastichy transition of type II*. A coefficient a_i in the continued fraction expansion of θ yields a_i parastichy transitions of type II. The occurence of a large coefficient a_i (and thus of many consecutive parastichy transitions of type II) is easy to detect visually: it leads to much less uniform point distributions in $\varphi_\theta(\mathbb{N})$. Figure 4 displays two examples.

The geometric construction of Section 5 shows the well-known fact that primary and secondary parastichies form two sets of spirals with opposite orientations if θ is irrational. Indeed, primary, respectively secondary, parastichies around $\varphi_\theta(n)$ are

defined by $\varphi_\theta(n \pm q_j)$, respectively by $\varphi_\theta(n \pm (q_{j-1} + kq_j))$ for suitable integers j, k, see Figure 2 where one has to think of $(0,0)$ as the point $\varphi_\theta(n)$ and of $\mathcal{L}$ as the ray defined by $\mathbb{R}_{>0}\varphi_\theta(n)$. (As always, q_{j-1} and q_j are denominators of convergents for θ.) The same integers j, k work for all n in some interval of large length compared to $\sqrt{n}$. The plane $\mathbb{R}^2$ is increasingly squeezed (for increasing n) in the direction of $\mathcal{L}$ and expanded in the orthogonal direction $\mathcal{L}^\perp$ in the construction of Section 5. This implies that parastichies of both kinds bend away from the rays issued by the origin. Moreover, there is exactly one parastichy family of larger, respectively of smaller slope than $\varphi_\theta(n)$ as can be seen by inspecting Figure 7.1. This explains the apparition of crisscrossing spirals in Figure 0.1. Secondary parastichy families are however no longer discernible (to the eye) for larger values of k, see Figure 7.3 where there are regions without obvious secondary parastichies. For irrational θ, they can however always be drawn "by continuity", if we start in suitable regions where no problems occur and if we push them forward using type II transition for (the projection of) γ_θ crossing the infinite boundary segment of $\mathcal{M}$.

7.1. **Transitions for parastichy families.** Transitions for parastichy families correspond to moments where the phyllotactic geodesic crosses the boundary $\partial\mathcal{M}$ of the fundamental domain for the modular curve. They occur on concentric circles. The boundary $\partial\mathcal{M}$ consists of a geodesic segment joining the square lattice (represented by $z = i$) to the regular hexagonal lattice (represented by $\frac{\pm 1+\sqrt{-3}}{2}$) and of a geodesic halfline issued from $\frac{\pm 1+\sqrt{-3}}{2}$ which recedes into the cusp of the modular curve. Intersections of the phyllotactic geodesic with (the image under $\mathrm{PSL}_2(\mathbb{Z})$ of) the shortest path joining the square lattice to the (regular) hexagonal lattice give rise to transitions of type I, intersection with the remining piece of $\partial\mathcal{M}$ to transitions of type II.

The number of "parallel" primary parastichy spirals forming a common family is always a denominator q_j of a convergent $\frac{p_j}{q_j} = [a_0; a_1, \dots, a_j]$ of the divergence angle $2\pi\theta = 2\pi[a_0, a_1, a_2, \dots]$. The number of secondary parastichy spirals in a common family is a denominator $q_j + kq_{j+1}, k \in \{0, 1, \dots, a_{j+2}\}$ of an intermediate convergent.

The exterior region of Figure 0.1 for example contains 55 primary parastichy spirals turning clockwise and 34 secondary parastichy spirals turning counterclockwise.

The evolution of the numbers of parastichy spirals (PS in the following table) can be described by:

	$\vdots$	$\vdots$	$\vdots$
I	q_{j-1} prim. PS q_{j-1} sec. PS	$\lvert\overline{\gamma_\theta(n)}\rvert \sim 1$	q_j sec. PS q_j prim. PS
II	$q_{j-1} + q_j$ sec. PS	$\lvert\Re(\overline{\gamma_\theta(n)}\rvert \sim \frac{1}{2}$	q_j prim. PS
II	$q_{j-1} + 2q_j$ sec. PS	$\lvert\Re(\overline{\gamma_\theta(n)}\rvert \sim \frac{1}{2}$	q_j prim. PS
II	$\vdots$	$\vdots$	$\vdots$
I	$q_{j-1} + a_{j+1}q_j = q_{j+1}$ sec. PS q_{j+1} prim. PS	$\lvert\overline{\gamma_\theta(n)}\rvert \sim 1$	q_j prim. PS q_j sec. PS
II	q_{j+1} prim. PS	$\lvert\Re(\overline{\gamma_\theta(n)}\rvert \sim \frac{1}{2}$	$q_j + q_{j+1}$ sec. PS
	$\vdots$	$\vdots$	$\vdots$

where $\overline{\gamma_\theta(n)}$ denotes a representant of of $\gamma_\theta(n)$ in $\mathcal{M}$.

(Families of) parastichy spirals exist to some extend in the real world (eg. in the approximate point set given by seeds of a real sunflower). Parastichy transitions

however are an ideal (or platonic) concept. They are somehow "smeared out" (like boundaries between adjacent colours of a rainbow) and cannot be localized exactly in a real flower.

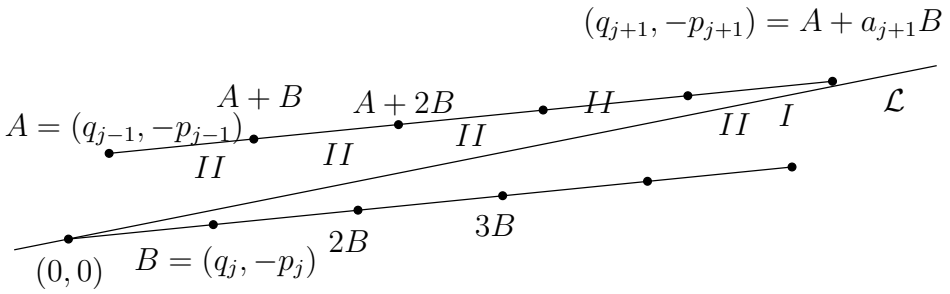

FIGURE 7.1. Parastichy transitions

Figure 7.1 attempts to illustrate the occurence of parastichy transitions using the geometric construction.

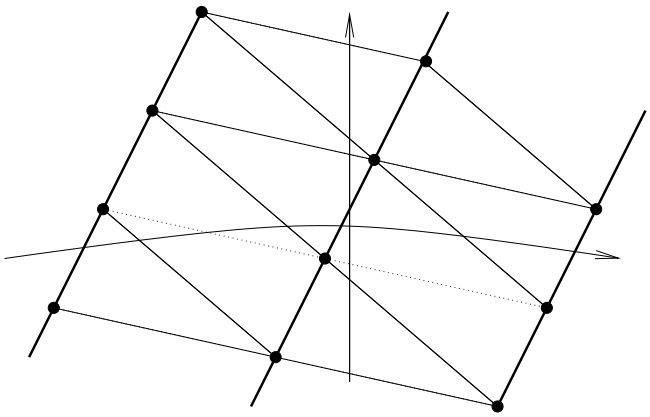

FIGURE 7.2. Death and birth of a family of secondary parastichy spirals

Figure 7.2 shows the death and birth of a family of secondary parastichy spirals corresponding to a value of n such that $|\Re(\overline{\gamma_\theta(n)}| \sim \frac{1}{2}$. The vertical arrow represents a ray issued from the origin. Primary parastichies are represented by fat segments, the dying family of secondary parastichies is drawn with dotted segments and the newborn family of secondary parastichies is given by ordinary segments. Turning around the origin on a circle of constant radius $\sim \sqrt{n}$ and counting the numbers a of primary parastichy spirals, b of dying secondary parastichies and c of newborn secondary parastichies, one gets the relation $c = a+b$. More precisely, the piecewise linear path involving only segments of primary and secondary dying parastichies giving the best approximation of the circle with radius $\sqrt{n}$ consists of b segments on primary parastichies and a segments on secondary parastichies. In order to work with the family of newborn parastichies, one has to replace every segment of the dying family by two segments, one from a primary parastichy and one from a newborn secondary parastichy. The number of segments on secondary parastichies (which is equal to the number of curves in the primary family) remains thus constant (and equals a) and the number c of segments on primary parastichies (which equals the number c of curves in the newborn secondary parastichy family) increases by a to $c = a + b$.

In order to prove that parastichy families are enumerated by denominators of (intermediate) convergents, it is now enough to remark that the assertion holds for

the final number of primary parastichies if θ is rational. A continuity argument implies the result in general.

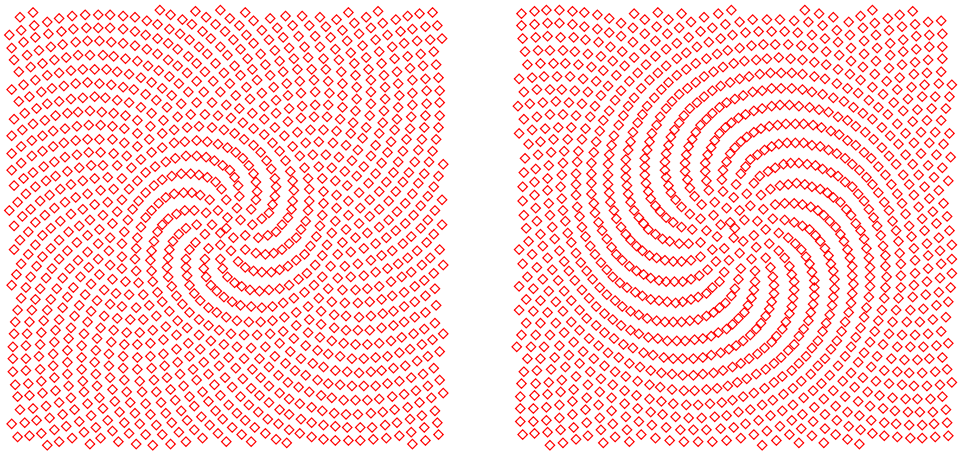

FIGURE 7.3. Small points of $\varphi_\theta(\mathbb{N})$ for $\theta = \frac{1765-\sqrt{5}}{2858}$ (left side) and $\theta = e^{-1}$ (right side).

The left half of Figure 7.3 shows all points of $\varphi_\theta(\mathbb{N})$ with real and imaginary parts smaller than 30 for $\theta = \frac{1765-\sqrt{5}}{2858}$ and $\theta = e^{-1}$. We have $\frac{1765-\sqrt{5}}{2858} = [0; 1, 1, 1, 1, 1, 1, 3, 1, 1, 1, 1, \dots]$ and the first convergents are

$$\frac{0}{1}, \frac{1}{1}, \frac{1}{2}, \frac{2}{3}, \frac{3}{5}, \frac{5}{8}, \frac{8}{13}, \frac{29}{47}, \frac{37}{60}, \dots .$$

The 13 parastichy spirals corresponding to the denominator 13 are clearly visible. This is of course due to the "large" coefficient 3 in the continued fraction expansion of θ which leads to three parastichy transitions of type II.

Similarly, we get for the parameter $\theta = e^{-1} = [0; 2, 1, 2, 1, 1, 4, 1, 1, 6, 1, 1, 8]$ corresponding to the right half of Figure 7.3 the convergents

$$\frac{0}{1}, \frac{1}{2}, \frac{1}{3}, \frac{3}{8}, \frac{4}{11}, \frac{7}{19}, \frac{32}{87}, \frac{39}{106}, \dots$$

with a clearly visible parastichy family corresponding to the denominator 19. This family is due to the large coefficient 4 (the family corresponding to 6 becomes visible at a larger scale) which causes four (visually imperceptible) parastichy transitions of type II.

7.2. **Monodromy.** One can consider two notions of monodromy for phyllotactic sets:

A first notion consists in moving a chosen basis for the local "lattice" by comparing bases of close points in the obvious way. No monodromy arises in this way: A closed loop gives rise to the identity.

A second, slightly more interesting feature is translational monodromy: going counterclockwise around the origin on a piecewise linear path and stitching the obtained lattice elements (with respect to "bases" which are "moved" continuously) together, we get at a point $a + ib \in \varphi_\theta(\mathbb{N})$ a vector close to $2\pi(-b + ia)$. More precisely, using a basis V_1, V_2 associated to primary and secondary parastichy spirals, this vector is of the form $(q_{j-1} + kq_j)V_1 \pm q_j V_2$ (with signs depending on the sign conventions for V_1 and V_2) if $\varphi_\theta(\mathbb{N})$ contains q_j primary and $(q_{j-1} + kq_j)$ secondary parastichy families at distance $\sqrt{a^2 + b^2}$ from the origin.

8. Combinatorics of Voronoi-diagrams

The material for this Section was motivated by empirical observations described and discussed in [12].

This Section presents geometric explanations of the observed features and describes a few related combinatorial facts.

8.1. **Voronoi-diagrams of complex lattices.** Voronoi cells of a complex lattice $\Gamma = \mathbb{Z} + \mathbb{Z}\tau$ corresponding to a complex number τ in the fundamental domain $\mathcal{M}$ defined by (A.1) yield a tiling of the plane $\mathbb{C} = \mathbb{R} + i\mathbb{R}$ with a fundamental domain given by the Voronoi cell of the origin. Voronoi domains are rectangles for $\tau = is \in \mathcal{M} \cap i\mathbb{R}$ and convex hexagons formed by three pairs of parallel opposite edges otherwise, i.e. if the real part of $\tau \in \mathcal{M}$ is non-zero.

There are thus only two possibilities for the combinatorics of the tiling defined by all Voronoi-cells of a complex lattice. They are illustrated by the square tiling obtained by covering the Euclidean plane with unit-squares centered at all points of $\mathbb{Z}^2$ and by the honeycomb-tiling consisting of regular hexagons.

We define the *Voronoi-diagram* of a discrete set $\mathcal{S}$ in an Euclidean plane $\mathbb{E}^2$ as the set of all points of $\mathbb{E}^2$ having at least two closest points in $\mathcal{S}$ at the same minimal distance. A Voronoi diagram is a plane graph with vertices given by points of $\mathbb{E}^2$ beeing closest to at least three points in $\mathcal{S}$. Edges are given by points of $\mathbb{E}^2$ equidistant to exactly two closest elements in $\mathcal{S}$. Voronoi cells are (not necessarily bounded) open convex polygons with a unique closest point in $\mathcal{S}$. They define connected components in the complement of the Voronoi diagram.

The combinatorics of a honeycomb diagram (or more generally of any reasonably locally finite Voronoi diagram involving only vertices of degree 3) are stable under small perturbations: Small independent perturbations of all points of a generic lattice corresponding to the honeycomb-case do not change the combinatorics of the Voronoi diagram. This does not hold for square (or rectangular) lattices: a small generic lattice-perturbation of a lattice $\mathbb{Z} + is\mathbb{Z}$ (for $s \geqslant 1$ a fixed real number) amounts to splitting all vertices of the grid-graph into two close adjacent vertices. For a continuous deformation $t \longmapsto \mathbb{Z} + \mathbb{Z}\tau(t)$ such that $\tau(0) = is$, $\Re(\tau(t)) < 0$, respectively $\Re(\tau(t)) > 0$, for $t < 0$, respectively for $t > 0$, one of the three pairs of opposite parallel edges in a Voronoi cell degenerates to an edge of length 0, the two other pairs of parallel edges become orthogonal. Combinatorially, we observe $I - H$ transformations which are applied simultaneously to all edges in one of the three families of parallel edges of the Voronoi-tiling, see Figure 8.1 for an illustration of a continuous lattice-deformation. There are thus two possibilities (illustrated by

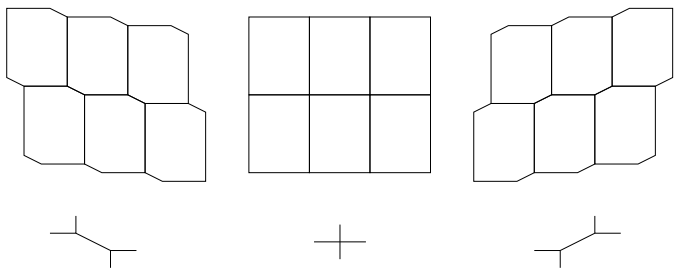

Figure 8.1. An $I - H$ transformation on Voronoi diagrams of lattices

Figure 8.1) for "resolving" vertices of degree 4 into pairs of vertices of degree 3 in a planar graph. Choosing for every vertex of the grid graph (with vertices $\mathbb{Z}^2$ and horizontal or vertical edges of unit length) one of the two possible resolutions yields a 3-regular planar graph with cells having at least 4 and at most 8 vertices. More

precisely, after separation of points with different resolutions by suitable "defect-curves", the resulting 3-regular graphs can be achieved as Voronoi-graphs of generic perturbations obtained by small vertical contractions and horizontal expansions, respectively horizontal contractions and vertical expansions, of the connected domains enclosed by defect curves (for unbounded domains one has to choose contractions-expansions which are asymptotically very close to the identity). This construction works of course for any grid-graph associated to a partial tiling of a subset of $\mathbb{R}^2$ by identical rectangles. Figure 8.2 shows an example: defect curves are dotted, points of the original grid-graph are replaced by short fat diagonal edges with mid-points given by the original lattice points and with endpoints joined in the obvious way by (almost) horizontal and vertical edges. Observe that the short fat diagonal edges are of length $O(\epsilon)$ in the Voronoi diagram of a generic perturbation of the set $\mathbb{Z}^2$ moving points less than ϵ. The remaining set of "non-short" or regular edges form a set of non-intersecting curves. These piece-wise linear curves formed by edges which are alternatingly almost horizontal, respectively almost vertical, form families of "parallel diagonals" in domains corresponding to the same type of resolution and are "orthogonal" (for an initial grid formed by squares) in two domains corresponding to different types of resolution. They change direction (by a quarter-turn) when crossing defect curves. Every Voronoi cell contains exactly 4 segments of such curves. Quadrilateral Voronoi cells (arising at suitable intersections of two defect curves) are enclosed by a unique closed curve consisting of four regular edges. Pentagons are almost enclosed by such a curve making a half-turn. Octogons are delimited locally by four different curves bending away from it.

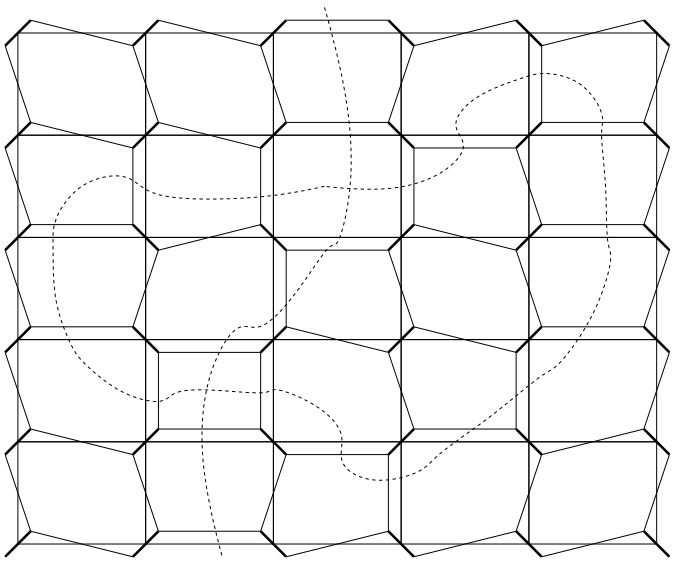

FIGURE 8.2. A generic perturbation of a rectangular tiling

In the case of a phyllotactic set $\varphi_\theta(\mathbb{N})$, the defect curves are asympotically given by circles with radii $\sqrt{\rho_i}$ associated to points $\gamma_\theta(\rho_i)$ of the phyllotactic geodesic corresponding to rectangular lattices (i.e. such that $\mathrm{PSL}_2(\mathbb{Z})\,(\gamma_\theta(\rho_i))$ intersects $i\mathbb{R}$). Since these circles have asymptotically large radii, defect curves are locally almost straight lines. Vonoroi cells intersecting a given defect curve form a chain with heptagons locally nearest to the origin paired to pentagons at locally maximal distance to the origin. Such "defect-dipoles" are joined by chains of "defect-hexagons" having two very small sides at distance 2 "pointing to the next pentagon" (non defectuous hexagons have approximatively parallel opposite sides of roughly equal lengths), see Figure 8.3 for a combinatorial illustration not respecting lengths (small

edges would be invisible otherwise) with a straight dashed line representing an ideal defect circle of infinite radius. The exterior of the defect circle is above the dashed line.

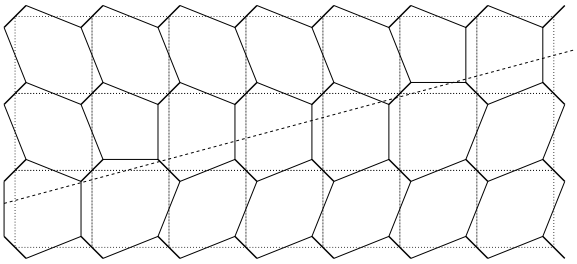

FIGURE 8.3. Local combinatorial situation near a defect circle

The numbers of defect hexagons and of defect dipoles are related in a straightforward way to the numbers of primary and secondary parastichy spirals. More precisely, if $\varphi_\theta(\mathbb{N})$ has a, respectively b, parastichy curves of the two possible types (primary, secondary) with $a < b$ at the defect circle, then the defect circle meets a defect pentagons and heptagons and $b-a$ defect hexagons. Primary and secondary parastichy spirals make up $\frac{2}{3}$ of all edges (corresponding to all "vertical" and "horizontal" edges of the unperturbed rectangular tiling represented by dotted lines in Figure 7) of the dual graph of the Voronoi-graph. The remaining edges of the Voronoi graph form "tertiary parastichy spirals" given by pairs of roughly opposite third-nearest points and running "in parallel" to the piecewise-linear curves formed by regular edges (and consisting alternatingly of "horizontal" and "vertical edges" in Figure 7).

Figure 1 of [12] is a picture in the case where θ is the golden mean. Two consecutive parastichy transitions of type II are always separated by a defect circle. Two parastichy transitions of type II separated by a parastichy transition of type I, are separated by either one or no defect circle. In the case $\theta = \frac{1+\sqrt{5}}{2}$ there is (asymptotically) always such a defect circle (which coincides almost with a parastichy transformation of type I) and defect-dipoles are separated at most by a unique defect-hexagon.

9. CHROMATIC PROPERTIES

A *Tait graph* is a 3-regular graph with 3-coloured edges such that three edges of all three edge-colours meet at every vertex. Plane Tait graphs are essentially the same as 4-coloured generic maps using the following classical trick. Identify the 3 edge-colours with the non-zero elements of Klein's Viergruppe $\mathbb{V} = \mathbb{Z}/2\mathbb{Z} \times \mathbb{Z}/2\mathbb{Z}$. Up to a colour-permutation, there is then a unique colouring with colours $\mathbb{V}$ such that adjacent regions coloured α and β are separated by an edge of colour $\alpha + \beta$.

Colouring parallel edges of the Voronoi-diagram (consisting of hexagons) of a generic lattice with three colours yields a Tait graph. The associated 4-colouring of the Voronoi-diagram has the property that the boundary of every non-defect hexagon meets all three other colours cyclically. Opposite parallel edges separate thus a given hexagon from two neighbours sharing the same colour. This colouring is unique up to colour-permutation and can be considered as a visualization of the morphism $\Lambda \longmapsto \mathbb{V} = \Lambda/2\Lambda$ sending a lattice Λ onto its reduction modulo 2. (Observe that the Voronoi diagram of the hexagonal lattice has also an essentially unique colouring involving only 3 colours associated to a suitable morphism from the hexagonal lattice into a cyclic group of order 3).

This Tait colouring (of the Voronoi diagram) exists of course for a generic radius of the phyllotactic set and can be extended uniquely to a Tait colouring of the

interior except at the boundary of the Voronoi-domain containing the origin. (Indeed, the situation at defect circles is quite easy to understand: there are "vertical", "horizontal" and very short (asymptotically infinitesimal) "defect" edges defining a coherent Tait-colouring which is unique up to colour-permutations.)

The Voronoi-domain of the phyllotactic set has thus a locally canonical 4-colouring (except at the origin) displaying chromatic monodromy when trying to extend this canonical colouring along a loop around the origin: Returning to the starting point we get a final colouring which is different. More precisely, the four colours get exchanged by pairs.

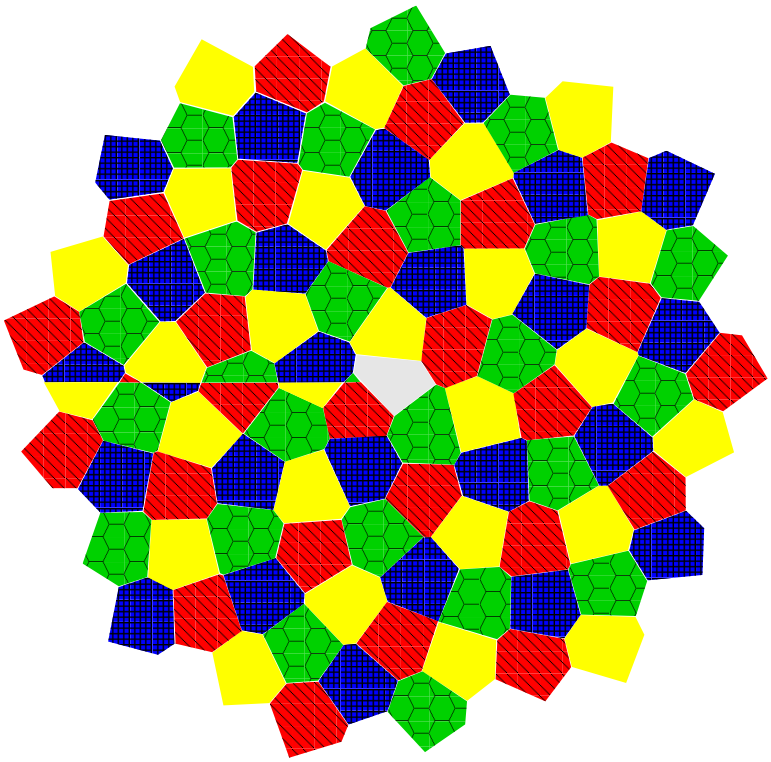

FIGURE 9.1. 4-colouring of the first Voronoi-cells for $\theta = \frac{1+\sqrt{5}}{2}$.

Figure 9.1 shows the canonical colouring with chromatic-monodromy concentrated at the real negative halfline.

A slightly different (but in fact equivalent) construction of this canonical local 4-colouring is as follows: Voronoi-cells of a lattice $\Lambda \subset \mathbb{C}$ are always 4-coloured using the homomorphism $\Lambda \longrightarrow \Lambda/2\Lambda \sim \mathbb{V}$. Affine lattice transformations preserving Λ induce affine transformations of the colour group $\mathbb{V}$. More precisely, a translation of Λ by an element $\lambda \notin 2\Lambda$ induces a translation of all colours in $\mathbb{V} \sim \Lambda/2\Lambda$ by the corresponding element $\lambda \pmod{2\Lambda}$. We get thus asymptotically a local 4-colouring of the phyllotactic set which is canonical up to addition of a constant in the colour group $\mathbb{V}$. Pushing the affine colour translations along a loop around the origin leads to the monodromy-translation of $\mathbb{V}$ partitioning $\mathbb{V}$ into two orbits of pairwise exchanged colours.

Colouring black and white the two monodromy-orbits of $\mathbb{V}$, we get a partition into black and white cells of all Voronoi-domains not containing the origin. Two adjacent black cells or two adjacent white cells are always separated by edges of the same "monodromy" colour associated to the monodromy translation of the colour-group $\mathbb{V}$. Figure 9.2 displays the associated black and white cells. Centers (i.e. elements of

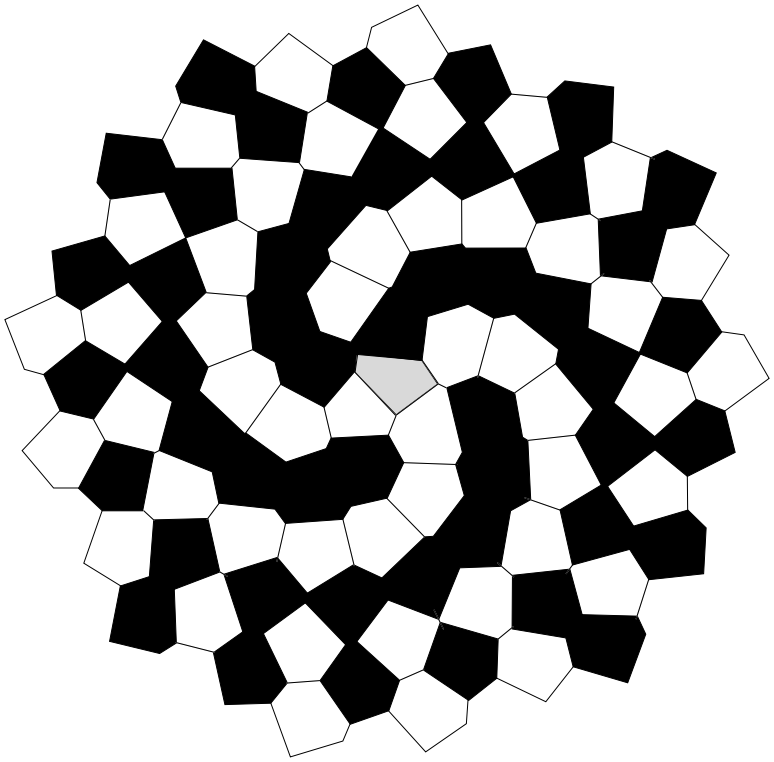

FIGURE 9.2. The black-white colouring obtained after identification of pairs of colours exchanged by monodromy.

the phyllotactic set defining the Voronoi-cells) of white cells correspond to images under the phyllotactic map φ_θ (with $\theta = \frac{1+\sqrt{5}}{2}$) of odd natural numbers. Centers of black cells correspond to images of non-zero even natural numbers. Black and white cells form stripes which degenerate at every third defect circles into a checkerboard-like situation. Indeed, defect circles are alternatingly associated to one of the three colours (colouring the asymptotically infinitesimal edges near the defect circle). At defect circles corresponding to the monodromy colour (i.e. where the edges of the monodromy colour degenerate into very short edges), the picture degenerates into a checkerboard. Elsewhere, we get alternating black and white "stripes" running (more or less) in parallel to a parastichy family. The total number of stripes (of both colours) is always an even Fibonacci number. The lower half of Figure 9.2 displays the situation for the even Fibonacci number 8 (the situation for the next even Fibonacci number, 34 is just visible at the boundary of the image). Since indices of consecutive even Fibonacci numbers in the Fibonacci sequence differ by 3 which is odd, two consecutive "stripy" regions rotate visually in opposite directions.

Choosing other pairwise identifications (orbits of $\mathbb{V}$ under addition of one of the other two non-zero elements of $\mathbb{V}$) of the four colours represented by $\mathbb{V}$ leads locally to stripy regions for other parastichy families. Every parastichy family can be represented locally in this way but there is of course a global error, accounted for by chromatic monodromy, if the number of curves in the family is odd. The birth-point and the dying point, corresponding to radially consecutive checkerboardy regions of such a family, are at every third defect circle. They correspond to the moment where the centers of adjacent black (or white) cells no longer correspond to pairs of third-nearest lattice points in the linearized lattice. They are thus birth-places (or grave-yards) for "tertiary" parastichy families which transform later during a type II transition into secondary parastichies.

The chromatic constructions described above work of course for many other real divergence angles: it is enough that the corresponding real number has a continued fraction expansion with coefficients not growing too fast. This ensures the existence of a (essentially unique) Tait colouring far from the origin. Near the origin, this Tait colouring breaks down. It gives however rise asymptotically to a local 4-coulouring (coming from the morphism $\Lambda \longrightarrow \Lambda/2\Lambda \sim \mathbb{V}$) of Voronoi-cells which displays in general a non-trivial colour-monodromy around the origin given by a monodromy translation (exchanging colours pairwise) in $\mathbb{V}$.

Remark 9.1. — Whorled phyllotaxis (see Section 10.3) of even order leads (for suitable divergence angles) to asymptotic Tait colourings with trivial colour-monodromy.

Remark 9.2. — Choosing a cyclic order on the edge-colours of a finite Tait graph yields a compact surface by gluing discs on all closed oriented paths defined by edges with the prescribed cyclical colour-scheme.

Defect lines give rise to genus proportional to a suitably defined combinatorial length. This gives in particular a topological interpretation of the 2-dimensional Ising model with periodic boundary conditions: The associated Hamiltonian (in the case of no external magnetic field) is proportional to the genus of the associated compact surface obtained by "opening" all vertices according to their sign. This leads to a canonical Tait graph allowing the construction of a compact surface. Since the resulting surface comes from a "fat graph" (also called "dessin d'enfants"), it has a natural complex structure, or equivalently, it has a Riemannian metric of constant curvature. The ordinary Ising model can thus be considered as the topological information (given by the genus) of a more general Ising model whose states define points in moduli spaces of compact Riemann surfaces. It would probably be interesting to have a better understanding of this generalized Ising model.

10. Other models

10.1. **Cylindric and logarithmic models.** In [3] Coxeter, following [2], models the structure of pineapples or pine-cones by approximating their shape with a cylinder which he develops on the plane thus getting an infinite strip of a lattice. The visible features (scales) on pineapples are the Voronoi cells of this lattice. The obtained lattice should stay close to the hexagonal lattice which has optimal packing and covering properties. Working with a cylinder of circumference 2π, we have thus to choose the optimal divergence angle $2\pi\theta$ such that the complex lattice $\mathbb{Z} + \mathbb{Z}(\theta + \epsilon i)$ is close to the hexagonal lattice for small ϵ. There is no exact control over the value of ϵ since pineapples or pine cones are not exact cylinders. We should thus choose the value of θ such that the geodesic $t \longmapsto \theta + ti$ is overall optimal for small positive ϵ. For a fixed value of θ, the map $\epsilon \longmapsto \theta + \epsilon i$ defines again a geodesic of the hyperbolic half-plane.

The best choice is of course again given by $\lambda = \frac{1+\sqrt{5}}{2}2\pi$ (or by its negative) modulo 2π yielding a geodesic which is asymptotically close to the shortest periodic geodesic

$$(0, \infty) \ni t \longmapsto \frac{1}{2}\frac{(1+it) + (-1+it)\sqrt{5}}{1+it}$$

of the modular curve $\mathrm{PSL}_2(\mathbb{Z})\backslash\mathbb{H}$.

Remark 10.1. — Identifying an infinitely long cylinder of circumference 1 with the quotient space of $\mathbb{C}$ under translations of the form $2i\pi\mathbb{Z}$, the usual exponential function transforms the cylindric model into the logarithmic model with points on a logarithmic ontogenetic spiral defined by $\mathbb{N} \ni n \longmapsto \rho^n e^{2i\pi\theta n}$.

10.2. **van Iterson's disc-packing model.** In [5] van Iterson considers periodic packings of equal discs on cylinders such that every disc touches (at least) two pairs of adjacent discs.

Levitov in [8] observes that the associated lattices correspond to elements of norm 1 in the modular domain and that the corresponding Teichmüller space (given by equivalence classes of lattices endowed with a positively-oriented basis) is a 3-regular tree with mid-edges given by the $\mathrm{PSL}_2(\mathbb{Z})$-orbit of i (corresponding to the square-lattice) and vertices given by the $\mathrm{PSL}_2(\mathbb{Z})$-orbit of $\frac{1+i\sqrt{3}}{2}$ (corresponding to the hexagonal lattice). The rooted subtree defined in the quarter-plane of $\mathbb{C}$ defined by all elements of $\mathbb{H}$ with non-negative real parts is then in natural bijection with the so-called Farey-tree. The optimal approximatively straight choice for a path on this rooted tree corresponds of course again to the golden mean and is given by alternating left- and right-turns at every bifurcation, as also observed by Levitov who gives a physical explanation based on energy levels of this fact.

Remark 10.2. — van Iterson's model involves sphere packings which are "locally optimal" in the sense that every disc of the packing (almost) touches four other discs. The associated Voronoi cells have however not asymptotically equal areæ.

The model determined by the phyllotactic map φ_θ gives Voronoi cells with asymyptotically equal areæbut leads to discs in the corresponding sphere packing which are almost all isolated. Exceptions are occuring at parastichy transitions of type I (happening asymptotically at the square lattice if θ is the golden ratio).

10.3. **Opposite and whorled phyllotaxis.** The content of this paper can be applied in a straightforward way to a whorled model of the sunflower: We consider a natural number $d \geqslant 2$ (the case $d = 2$ is called "opposite phyllotaxis", the case $d > 3$ "whorled phyllotaxis" in botanics) and we denote by $\mathbb{U}_d$ the set of all d complex d-th roots of 1 given by the zeros of the polynomial $z^d - 1$. The set $\mathbb{U}_d\varphi_\theta\left(\frac{1}{d}\mathbb{N}\right)$ defined by the map

$$\mathbb{U}_d \times \mathbb{N} \ni (\omega, n) \longmapsto \omega\sqrt{\frac{n}{d}}e^{2i\pi\theta n/d}$$

(invariant under the obvious isometrical action defined by the multiplicative subgroup $\mathbb{U}_d$ of $\mathbb{C}^*$) is then locally essentially a rescaling by a factor $\frac{1}{d}$ (followed by a rotation) of the phyllotactic set $\varphi_\theta(\mathbb{N})$. Up to reparametrization (replacing t with td), it admits the same phyllotactic geodesic. Numbers of parastichy curves in a given family are simply multiplied by d with respect to the corresponding number in $\varphi_\theta(\mathbb{N})$.

11. Testing the existence of phyllotactic geodesics in real sunflowers

Phyllotactic geodesic are perhaps a mere mathematical artefact due to the use of the model maps φ_θ. This Section sketches a test probing the reality of the theory.

A first step is of course gathering real data, consisting of a fair number of pictures of large flawless sunflower-capitula. These pictures should be enriched by adding as smoothly as possible (using perhaps splines or trigonometric functions and a least square method) all visible parastichy spirals. Intersections of transversal parastichy spirals should now be taken as the centers of seeds. Points near the center can be neglected.

We can check adequacy of $\varphi_\theta(\mathbb{N})$ for sunflowers as follows: Determine for each picture (endowed with a complex coordinate system) parameters $A \in \mathbb{C}, C \in \mathbb{C}^*, \theta, \gamma \in \mathbb{R}$ giving the best least square approximation of the obtained seed-centers with a suitable set of points of the form

$$\mathbb{N} \ni n \longmapsto A + C\sqrt{n+\gamma}\; e^{2i\pi\theta n},$$

supposing that the pictures have no distorsions (additional parameters are necessary otherwise). If this approximation is nearly perfect, the sunflower map is an accurate description of reality and the existence of phyllotactic geodesics is confirmed. A failure or a bad match does however not contradict the existence of phyllotactic geodesics but forces us to compute points of "hypothetical" geodesics using the real data-sets instead of the model set $\varphi_\theta(\mathbb{N})$.

This can be achieved as follows: For each point P neither on the boundary nor in the center of the sunflower, we determine pairs of points a, A and b, B adjacent to P with a, A on one parastichy spiral through P and b, B on the other, transversal parastichy spiral through P. The linearized lattice at P is then approximatively given by $\mathbb{Z}\frac{A-a}{2}+\mathbb{Z}\frac{B-b}{2}$. This allows the computation of the corresponding modular invariant by considering the point of the modular curve represented by $\pm\frac{A-a}{B-b}$ (for the unique sign choice leading to a strictly positive imaginary part). Suitable lifts of these points to $\mathbb{H}$ should now lie close to a hyperbolic geodesic which can be guessed by least square approximation.

Appendix A. Complex lattices and hyperbolic geometry

For the convenience of the reader, we recall a few elementary and well-known facts first of the theory of lattices, following closely parts of Section 2.2 in Chapter VII of [14], then of hyperbolic geometry, see for example [1].

A.1. **Lattices of $\mathbb{C}$.** A *lattice* in $\mathbb{C}$ is a free additive subgroup generated by two $\mathbb{R}$-linearly independent elements ω_1, ω_2 of $\mathbb{C}$. In the sequel, we consider lattices only up to orientation-preserving similarities. Two lattices Γ and Λ of $\mathbb{C}$ are thus equivalent if $\Lambda = \lambda\Gamma$ for some non-zero constant $\lambda \in \mathbb{C}^*$. Given a basis ω_1, ω_2 of a lattice $\Gamma = \mathbb{Z}\omega_1 + \mathbb{Z}\omega_2$, we consider $z = \frac{\omega_1}{\omega_2}$. Up to replacing, say, ω_1 by $-\omega_1$, we can suppose that the imaginary part $y = \Im(z)$ of $z = x + iy$ is strictly positive.

Thus, a lattice $\mathbb{Z}\omega_1 + \mathbb{Z}\omega_2 = \left(\mathbb{Z} + \mathbb{Z}\frac{\omega_1}{\omega_2}\right)\omega_2$ is equivalent to the lattice $\Gamma(z) = \mathbb{Z} + \mathbb{Z}z$ generated by 1 and by the element $z = \frac{\omega_1}{\omega_2}$ of the open upper half-plane $\mathbb{H} = \{z \in \mathbb{C} \mid \Im(z) > 0\}$.

Given an unimodular integral matrix $g = \begin{pmatrix} a & b \\ c & d \end{pmatrix} \in \mathrm{SL}_2(\mathbb{Z})$, the quotient

$$z' = \frac{\omega_1'}{\omega_2'} = \frac{a\omega_1 + b\omega_2}{c\omega_1 + d\omega_2} = \frac{a\frac{\omega_1}{\omega_2} + b}{c\frac{\omega_1}{\omega_2} + d}$$

associated to the basis $\omega_1' = a\omega_1 + b\omega_2$, $\omega_2' = c\omega_1 + d\omega_2$ of a lattice $\mathbb{Z}\omega_1 + \mathbb{Z}\omega_2$ is obtained from $z = \frac{\omega_1}{\omega_2}$ by the usual action $g.z = \frac{az+b}{cz+d}$ of the modular group $\mathrm{PSL}_2(\mathbb{Z}) = \mathrm{SL}_2(\mathbb{Z})/\pm\mathrm{Id}$ on $\mathbb{H}$.

Hence the map $\mathbb{Z}\omega_1 + \mathbb{Z}\omega_2 \longmapsto z = \frac{\omega_1}{\omega_2} \in \mathbb{H}$ induces a one-to-one correspondence between equivalence classes $\mathbb{C}^*\Gamma$ of lattices and points of the modular curve $\mathrm{PSL}_2(\mathbb{Z})\backslash\mathbb{H}$, see Chapter VII, Proposition 2 and Proposition 3 of [14]. A fundamental domain for the action of the modular group $\mathrm{PSL}_2(\mathbb{Z})$ on $\mathbb{H}$ is given by the *fundamental domain*

$$\mathcal{M} = \left\{ z \in \mathbb{C} \mid |z| \geqslant 1 \text{ and } |\Re(z)| \leqslant \frac{1}{2} \right\} \tag{A.1}$$

for $\mathrm{PSL}_2(\mathbb{Z})\backslash\mathbb{H}$. Two elements z_1, z_2 of $\mathcal{M}$ represent the same equivalence-class of lattices if and only if either $z_2 = -\frac{1}{z_1}$ or $z_2 = z_1 \pm 1$. The *modular curve* $\mathrm{PSL}_2(\mathbb{Z})\backslash\mathbb{H} = \mathcal{M}/\sim$ is a complex orbifold with two conical points represented by $\frac{-1+i\sqrt{3}}{2}$ (of angle $\frac{2\pi}{3}$ and corresponding to regular hexagonal lattices) and by i (of angle π and corresponding to square lattices) and with a cusp (corresponding to a neighbourhood of the degenerate case of an additive subgroup of rank 1 in $\mathbb{C}$).

An *affine lattice* is a coset $\alpha + \Gamma$ obtained by translating a complex lattice $\Gamma \subset \mathbb{C}$ by some vector $\alpha \in \mathbb{C}$. We consider affine lattices only up to orientation-preserving affine similarities. Equivalence classes of affine lattices are also in one-to-one correspondence with elements of the modular curve $\mathrm{PSL}_2(\mathbb{Z})\backslash\mathbb{H}$.

A.2. **Hyperbolic geometry on the Poincaré half-plane.** We recall a few facts concerning the hyperbolic Poincaré half-plane $\mathbb{H}$, see [1] for an elementary introduction to hyperbolic geometry.

The upper half-plane $\mathbb{H} = \{z \in \mathbb{C} \,|\Im(z) > 0\}$ can be turned into a real hyperbolic simply connected Riemannian manifold of dimension 2 and of constant curvature -1 by equipping it with the Riemannian metric $(ds)^2 = \frac{dx^2+dy^2}{y^2}$ at a point $z = x + iy \in \mathbb{H}$. The *Poincaré half-plane* is the hyperbolic manifold (still denoted by) $\mathbb{H}$ obtained in this way.

The group of all orientation-preserving isometries of the Poincaré half-plane is given by the set of all Möbius transformations

$$z \longmapsto \begin{pmatrix} a & b \\ c & d \end{pmatrix} z = \frac{az+b}{cz+d}$$

defined by matrices $\begin{pmatrix} a & b \\ c & d \end{pmatrix}$ in $\mathrm{SL}_2(\mathbb{R})$, respresenting elements in $\mathrm{PSL}_2(\mathbb{R}) = \mathrm{SL}_2(\mathbb{R})/\pm\mathrm{Id}$.

Geodesics of $\mathbb{H}$ are half-circles (with respect to the usual Euclidean metric of $\mathbb{C}$) centered at the boundary $\mathbb{R}$ of $\mathbb{H} \subset \mathbb{C}$ or halflines $\{a + iy \in \mathbb{C} \mid y > 0\} \subset \mathbb{H}$ perpendicular to $\mathbb{R}$.

An orientation-preserving isometry ι of the Poincaré half-plane is *hyperbolic* if it acts by translation on an invariant geodesic. A Möbius transformation associated to $\begin{pmatrix} a & b \\ c & d \end{pmatrix} \in \mathrm{SL}_2(\mathbb{R})$ defines a hyperbolic isometry ι if and only if $|a + d| > 2$. The invariant geodesic of ι is given by the halfcircle in $\mathbb{H}$ delimited by the two real points $\frac{a-d\pm\sqrt{(d-a)^2+4bc}}{2c}$ if $c \neq 0$ respectively by the halfline $\{b/(d-a)+iy \mid y > 0\}$ otherwise.

Lemma A.1. — *For* $\begin{pmatrix} a & b \\ c & d \end{pmatrix} \in \mathrm{GL}_2(\mathbb{R})$ *with* $cd \neq 0$ *and positive determinant* $ad - bc > 0$, *the image of the map from* $\mathbb{R}_{>0} = (0, +\infty)$ *into* $\mathbb{C}$ *defined by*

$$t \longmapsto \frac{ait+b}{cit+d}$$

is an open half-circle of $\mathbb{H}$ *centered on* $\frac{ad+bc}{2cd}$ *with radius* $\left|\frac{ad-bc}{2cd}\right|$ *(with respect to the Euclidean norm* $\| z \| = \sqrt{x^2+y^2}$ *for* $z = x + iy \in \mathbb{C}$*).*

Proof. — Möbius transformations preserve geodesics of $\mathbb{H}$. Thus the Möbius transformation defined by the matrix $\begin{pmatrix} a & b \\ c & d \end{pmatrix}$ sends the geodesic $\{ti \mid t > 0\} \subset \mathbb{H}$ onto a geodesic of $\mathbb{H}$ with finite boundary points given by $\frac{b}{d}$ (corresponding to $t = 0$) and $\frac{a}{c}$ (corresponding to $t = +\infty$). This geodesic is the open halfcircle (for the usual Euclidean metric of $\mathbb{C}$) of the upper halfplane with center $\frac{1}{2}\left(\frac{b}{d} + \frac{a}{c}\right) = \frac{ad+bc}{2cd}$ and diameter $\left|\frac{a}{c} - \frac{ad+bc}{2cd}\right| = \left|\frac{ad-bc}{2cd}\right|$. □

Remark A.2. — Lemma A.1 is equivalent to the identity

$$\left(\frac{act^2+bd}{c^2t^2+d^2} - \frac{ad+bc}{2cd}\right)^2 + \left(\frac{ad-bc}{c^2t^2+d^2}\right)^2 t^2 = \left(\frac{ad-bc}{2cd}\right)^2 .$$

Appendix B. Basics for continued fractions

We denote by $[a_0; a_1, a_2, \dots]$ the continued fraction expansion

$$\theta \quad = \quad a_0 + \cfrac{1}{a_1 + \cfrac{1}{a_2 + \ddots}} \ ,$$

of a real number θ. The coefficients $a_0, a_1, \dots$ are recursively defined by $a_i = \lfloor \theta_i \rfloor$ where $\theta_0 = \theta$ and $\theta_n = \frac{1}{\theta_{n-1} - a_{n-1}} = \frac{1}{\{\theta_{n-1}\}}$ if $\theta_{n-1} \notin \mathbb{Z}$, respectively by $\theta_n = 0$ if $\theta_{n-1} \in \mathbb{Z}$. The coefficient a_0 of a continued fraction expansion can be an arbitrary integer (positive, zero or negative). $a_1, a_2, \dots$ are either all strictly positive or they start with a finite number of strictly positive integers followed by an infinite string of zeros. The last case arises if and only if θ is rational. The sequence $a_0, a_1, \dots$ is infinite and ultimately periodic with non-zero period if and only if $\mathbb{Q}[\theta]$ is a quadratic number field. Every irrational number has a unique continued fraction expansion. Rational numbers have two expansions given by $[a_0; a_1, \dots, a_m, 1]$ and $[a_0; a_1, \dots, a_m + 1]$ for suitable integers $m \geqslant 0,\ a_0 \in \mathbb{Z},\ a_1, \dots, a_m \geqslant 1$.

We have the continued fraction expansions

$$\theta_n \quad = \quad [a_n; a_{n+1}, a_{n+2}, a_{n+3}, \dots] \tag{B.1}$$

for all $n \in \mathbb{N}$. *Convergents* for

$$\theta = \theta_0 = a_0 + \cfrac{1}{a_1 + \cfrac{1}{a_2 + \ddots}}$$

are rational numbers of the form

$$\frac{p_{-2}}{q_{-2}} = \frac{0}{1},\ \frac{p_{-1}}{q_{-1}} = \frac{1}{0}, \frac{p_n}{q_n} = \frac{p_{n-2} + a_n p_{n-1}}{q_{n-2} + a_n q_{n-1}} = [a_0; a_1, \dots, a_n],\ n \geqslant 0$$

and can also be define by $\frac{p_n}{q_n} = [a_0; a_1, \dots, a_n]$, see Theorem 149 in [4]. *Intermediate convergents* are given by

$$\frac{p_{n-2} + k p_{n-1}}{q_{n-2} + k q_{n-1}},\ k \in \{0, \dots, a_n - 1\} \ .$$

The easy identity

$$p_{n-1} q_n - p_n q_{n-1} = (-1)^n \tag{B.2}$$

(see Theorem 150 in [4] or Theorem 2 in [7]), equivalent to $\frac{p_{n-1}}{q_{n-1}} - \frac{p_n}{q_n} = \frac{(-1)^n}{q_{n-1} q_n}$, implies

$$\frac{p_{2n}}{q_{2n}} < \frac{p_{2n+2}}{q_{2n+2}} < \dots < \theta < \dots < \frac{p_{2n+1}}{q_{2n+1}} < \frac{p_{2n-1}}{q_{2n-1}} \ .$$

This shows

$$\left| \theta - \frac{p_n}{q_n} \right| < \frac{1}{a_{n+1} q_n^2} \tag{B.3}$$

and ensures that convergents are excellent rational approximations of an irrational number.

Acknowledgements

I would like to thank David Speyer who started my interest in phyllotaxis by proposing $\varphi_\theta(\mathbb{N})$ as an interesting configuration to consider in relation with Question 3307 of Mathoverflow, see [9], Tanguy Rivoal who prompted me to write up the details, Pierre de la Harpe and Etienne Ghys for useful remarks and comments.

This work has been partially supported by the LabEx PERSYVAL-Lab (ANR–11-LABX-0025). The author is a member of the project-team GALOIS supported by this LabEx.

References

[1] J.W. Anderson. *Hyperbolic Geometry*, Springer, 2005.

[2] L. and A. Bravais. Essai sur la disposition des feuilles curvisériées, *Ann. Sci. Naturelles (2)*, 7:42–110, 1837.

[3] H.S.M. Coxeter. The role of intermediate convergents in Tait's explanation for phyllotaxis, *J. of Alg.*, 20:167–175, 1972.

[4] G.H. Hardy, E.M. Wright. *An Introduction to the Theory of Numbers*, Oxford University Press, 1960 (fourth edition).

[5] G. van Iterson. *Mathematische und mikroskopisch-anatomische Studien über Blattstellungen nebst Betrachtungen über den Schalenbau der Miliolinen*, Gustav Fischer, Jena, 1907.

[6] R.V. Jean, D. Barabé (editors). *Symmetry in Plants*, Series in Mathematical Biology and Medecine, vol. 4, World Scientific, 1998.

[7] A. Ya. Khinchin. *Continued fractions*, The University of Chicago Press, Chicago, 1964.

[8] L.S. Levitov. Energetic Approach to Phyllotaxis, *Europhys. Lett.*, 6:533–539, 1991.

[9] Mathoverflow: http://mathoverflow.net/questions/3307/can-a-discrete-set-of-the-plane-of-uniform-density-intersect-all-large-triangles.

[10] R.V. Jean, D. Barabé (editors). *Symmetry in plants*, World Sci. Publishing, River Edge, NJ, 1998.

[11] F. Rothen, A.-J. Koch. Phyllotaxis, or the properties of spiral lattices. I Shape invariance under compression, *J. Phys. France*, 50:633–657, 1989.

[12] J-F. Sadoc, J. Charvolin, N. Rivier. Phyllotaxis: a non conventional solution to packing efficiency in situations with radial symmetry, *Acta Cryst. A*, 68:470–483, 2012.

[13] C. Series. The Geometry of Markoff Numbers, *Math. Int.*, 7(3):20–29, 1985.

[14] J-P. Serre. *Cours d'arithmétique*, Presses Universitaires de France, 1970.

[15] D.W. Thompson. *On Growth and Form*, Dover reprint (1992) of second ed. (1942) (first ed. 1917).

[16] H. Vogel. A better way to construct the sunflower head, *Math. Biosc.*, 44:179–189, 1979.

Manuscript received February 7, 2013,
revised June 19, 2014,
accepted June 24, 2014.

Roland BACHER
Université Grenoble Alpes, Institut Fourier (CNRS UMR 5582), 38000 Grenoble, France
roland.bacher@ujf-grenoble.fr